REPORT DOCUMENTATION PAGE

Form Approved
OMB No. 0704-0188

PLEASE DO NOT RETURN YOUR FORM TO THE ABOVE ADDRESS.

1. REPORT DATE *(DD-MM-YYYY)*	2. REPORT TYPE	3. DATES COVERED *(From - To)*
01-12-2003	N/A	15-May-2002 - 14 May 2004

4. TITLE AND SUBTITLE

Final Technical Report for Analytical Assessments Related to Microbubble Drag Reduction

5a. CONTRACT NUMBER

N/A

5b. GRANT NUMBER

N00014-02-1-0574

5c. PROGRAM ELEMENT NUMBER

N/A

6. AUTHOR(S)

M. A. Ebadian, Ph.D

5d. PROJECT NUMBER

09130

5e. TASK NUMBER

01

5f. WORK UNIT NUMBER

03300

7. PERFORMING ORGANIZATION NAME(S) AND ADDRESS(ES)

Hemispheric Center for Envionmental Technology
Florida International University
10555 West Flagler Street, EC 2100
Miami, FL 33174

8. PERFORMING ORGANIZATION REPORT NUMBER

N/A

9. SPONSORING/MONITORING AGENCY NAME(S) AND ADDRESS(ES)

Mr. Patrick Purtell
Office of Naval Research
800 North Quincy Street
Arlington, VA 22217

10. SPONSOR/MONITOR'S ACRONYM(S)

ONR 333

11. SPONSOR/MONITOR'S REPORT NUMBER(S)

N/A

12. DISTRIBUTION/AVAILABILITY STATEMENT

Distribution is unlimited.

13. SUPPLEMENTARY NOTES

N/A

14. ABSTRACT

In this project, the Hemispheric Center for Environmental Technology (HCET) at Florida International University has conducted computational studies of the microbubble drag reduction mechanism. The objective of this research was to assess the roles of mixture density variation and surface roughness in microbubble drag reduction.
This research was carried out in collabration with the Applied Research Laboratory at the Penn State University, where substantial experimental research and theoretical understanding and modeling research have been conducted in this area. The principal work scope was carried out by HCET with ARL providing data and guidance and recommending models and analysis tools to support the research.

15. SUBJECT TERMS

N/A

16. SECURITY CLASSIFICATION OF:			17. LIMITATION OF ABSTRACT	18. NUMBER OF PAGES	19a. NAME OF RESPONSIBLE PERSON
a. REPORT	b. ABSTRACT	c. THIS PAGE			Robert F. Kunz
U	U	U	U	22	19b. TELEPHONE NUMBER *(Include area code)* 814-865-2144

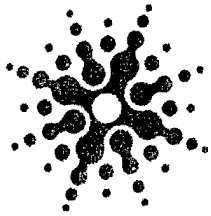

HCET Hemispheric Center for Environmental Technology
environment • energy • information technology

Final Technical Report
for Analytical Assessments Related to Microbubble Drag Reduction

December 2003

Prepared Under

Subrecipient Agreement S03-15

Submitted to

Applied Research Laboratory
The Pennsylvania State University

Submitted by

M. A. Ebadian, Ph.D.
Hemispheric Center for Environmental Technology
Florida International University
10555 West Flagler Street, EC 2100
Miami, FL 33174
Phone: (305) 348-4238
Fax: (305) 348-4176
E-mail: ebadian@hcet.fiu.edu

Team Members

P. V. Skudarnov, Ph.D.
C. X. Lin, Ph.D.
G. P. Philippidis, Ph.D.

December 31, 2003

TABLE OF CONTENTS

LIST OF FIGURES AND TABLES

1.0 INTRODUCTION

An increase in range or speed of the U.S. Navy's surface vessels, submarines, underwater vehicles, and weapons can be achieved by reducing the skin friction drag of these objects. Microbubble drag reduction (MDR) is a unique flow control technique that employs injection of gas into a liquid turbulent boundary layer to form microbubbles that can dramatically reduce the skin friction drag. This technique, which is able to provide drag reductions of as much as 80%, offers great potential in Naval applications.

McCormick and Bhattacharya (1973) reported the first microbubble drag reduction experiments. During the past decades, many research efforts have been devoted to microbubble drag reduction (Merkle and Deutsch 1992). The work conducted by researchers in the former Soviet Union and in the United States, primarily by the Applied Research Laboratory (ARL) at The Pennsylvania State University, provided the benchmark in microbubble drag reduction research. It has been found that there are many factors that influence microbubble drag reduction, including air jet flow rate, injection process, free stream velocity, pore size, buoyancy, and surface configuration. As evidenced by published papers in the open literature, most of the previous studies of microbubble drag reduction were conducted experimentally. Due to the complexity of the microbubble boundary layers, theoretical investigations have fallen behind the progress made by experimental studies. It is recognized that a better understanding of the microbubble drag reduction mechanism is critical to its optimal performance with minimal use of gas volume in practical applications.

In recent years, analytical computational modeling of microbubble drag reduction has been attempted by several researchers (Madavan et al. 1985; Marie 1987; Kim and Cleaver 1995; Meng and Uhlman 1998; Xu et al. 2002; Kunz et al. 2003) to reveal the mechanism of the microbubble drag reduction phenomenon. A study by Legner (1984) proposed a simple stress model for gas bubble drag reduction and indicated that the drag reduction was caused by a combination of density reduction and turbulence modification. Meng and Uhlman (1998) suggested that bubble splitting was a plausible basic mechanism for reducing turbulence in a microbubble-laden turbulent boundary layer. These efforts made impressive progress toward the in-depth understanding of the mechanism from various angles. However, the available theoretical work is not sufficient to answer all the questions associated with microbubble drag reduction. The relative importance of postulated mechanisms remains unclear. One issue of specific interest is bubble breakup during microbubble drag reduction, which can give rise to turbulence attenuation. It has also been suggested that a simple density effect is the dominant source of drag reduction. Very recent experiments at ARL have also shown that significantly more drag reduction can be obtained on rough surfaces than on smooth surfaces with microbubble drag reduction. It is not understood why this phenomenon occurs.

In this project, the Hemispheric Center for Environmental Technology (HCET) at Florida International University has conducted computational studies of the microbubble drag reduction mechanism. The objective of this research was to assess the roles of mixture density variation and surface roughness in microbubble drag reduction.

This research was carried out in collaboration with the Applied Research Laboratory at The Penn State University, where substantial experimental research and theoretical understanding and modeling research have been conducted in this area. The principal work scope was carried out by HCET with ARL providing data and guidance and recommending models and analysis tools to support the research.

2.0 NUMERICAL MODEL

During this project, computational assessment of the role of mixture density variation in microbubble drag reduction was carried out. To perform this assessment, a two-dimensional computational fluid dynamics (CFD) model of microbubble-laden flow over a flat plate was developed. The model consisted of Reynolds-averaged Navier-Stokes (RANS) transport equations and a standard k-ω turbulence model (Wilcox 1998) with a low Reynolds number correction. This model was designed to be applied throughout the boundary layer when the near wall mesh is sufficiently fine. The RANS transport equations are

$$\frac{\partial \rho}{\partial t}+\frac{\partial}{\partial x_i}(\rho u_i)=0 \tag{1}$$

$$\frac{\partial}{\partial t}(\rho u_i)+\frac{\partial}{\partial x_j}(\rho u_i u_j)=-\frac{\partial p}{\partial x_i}+\frac{\partial}{\partial x_j}\left[\mu\left(\frac{\partial u_i}{\partial x_j}+\frac{\partial u_j}{\partial x_i}-\frac{2}{3}\delta_{ij}\frac{\partial u_l}{\partial x_l}\right)\right]+\frac{\partial}{\partial x_j}\left(-\rho\overline{u_i' u_j'}\right) \tag{2}$$

The last term in equation (2) is called Reynolds stresses and is related to mean velocity gradients using Boussinesq hypothesis:

$$-\rho\overline{u_i' u_j'}=\mu_t\left(\frac{\partial u_i}{\partial x_j}+\frac{\partial u_j}{\partial x_i}\right)-\frac{2}{3}\left(\rho k+\mu_t\frac{\partial u_i}{\partial x_i}\right)\delta_{ij} \tag{3}$$

The transport equations for the turbulence kinetic energy k and the specific dissipation rate ω are

$$\frac{\partial}{\partial t}(\rho k)+\frac{\partial}{\partial x_i}(\rho k u_i)=\frac{\partial}{\partial x_j}\left(\Gamma_k\frac{\partial k}{\partial x_j}\right)+G_k-Y_k \tag{4}$$

$$\frac{\partial}{\partial t}(\rho \omega)+\frac{\partial}{\partial x_i}(\rho \omega u_i)=\frac{\partial}{\partial x_j}\left(\Gamma_\omega\frac{\partial \omega}{\partial x_j}\right)+G_\omega-Y_\omega \tag{5}$$

where Γ_k and Γ_ω are the effective diffusivity of k and ω, respectively; G_k is the generation of turbulence kinetic energy due to mean velocity gradients; G_ω is the generation of ω; and Y_k and Y_ω are the dissipation of k and ω due to turbulence.

The low Reynolds number correction is achieved by introducing damp coefficient α^* into the turbulent viscosity equation as shown below:

$$\mu_t=\alpha^*\frac{\rho k}{\omega} \tag{6}$$

$$\alpha^*=\alpha_\infty^*\left(\frac{\alpha_0^*+\mathrm{Re}_t/R_k}{1+\mathrm{Re}_t/R_k}\right) \tag{7}$$

where $\alpha_\infty^* = 1$; $\quad \mathrm{Re}_t = \frac{\rho k}{\mu \omega}$; $\quad R_k = 6$; $\quad \alpha_0^* = \frac{\beta_i}{3}$; $\quad \beta_i = 0.072$

Wall boundary condition for the turbulence kinetic energy is

$$\frac{\partial k}{\partial n} = 0 \tag{8}$$

where n is the local coordinate normal to the wall.

Wall boundary condition for the specific dissipation rate is discussed in detail in section 4.0, where the effect of surface roughness on microbubble drag reduction is addressed.

Mixture density variation due to microbubbles was modeled by introducing CO_2 gas species and using the species transport model. In the species transport model, the local mass fraction of each species, Y_i, is predicted by solving a convection-diffusion equation for the ith species:

$$\frac{\partial}{\partial t}(\rho Y_i) + \nabla \cdot (\rho \vec{v} Y_i) = -\nabla \cdot \vec{J}_i + R_i + S_i \tag{9}$$

where $\vec{J}_i$ is the diffusion flux of species i, R_i is the net rate of production of species i by chemical reaction ($R_i = 0$ in this case), and S_i is the rate of creation from any sources. For turbulent flows such as those considered here, the diffusion flux has the following form:

$$\vec{J}_i = -\left(\rho D_{i,m} + \frac{\mu_t}{Sc_t} \right) \nabla Y_i \tag{10}$$

where Sc_t is the turbulent Schmidt number, μ_t is the turbulent viscosity, and $D_{i,m}$ is the diffusion coefficient for species i in the mixture.

The CO_2 gas was introduced as species mass source in the first layer of cells along the porous section of the flat plate ("Wall 2" on Figure 1). Zero-gradient condition for all species was used on the flat plate. Mixture density was computed using the volume-weighted mixing law. This model does not capture the physics of the microbubbles; however, it allows one to ascertain whether a simple mixture density variation effect is the dominant source of microbubble drag reduction. The model was solved using the FLUENT 6 CFD solver.

A 712 mm by 250 mm computational domain (Figure 1) with 112 x 64 grid points (Figure 2) was used to solve the model. The height of the computational domain was selected so that it would be at least 20 turbulent boundary layer thicknesses, which, for the present case, was about δ = 10 mm. Wall-normal clustering of cells was used to resolve the boundary layer, and axial clustering was used near the ends of flat plate sections. Dimensions of the computational domain and boundary conditions are shown schematically in Figure 1. Constant velocity boundary condition is used in the domain inlet, symmetry boundary conditions are used in the leading part of the domain as well as in the far field above the flat plate, no slip boundary condition is applied at the flat plate, and constant pressure boundary condition is applied at the domain outlet. Values of k and ω at the domain inlet were specified as 1.2×10^{-5} m^2/s^2 and 1.2×10^{-3} s^{-1}, respectively. The

same values were used as initial guesses for k and ω. To compute gas inlet volumetric flow rates, the depth of the domain was assumed to be 102 mm. The dimensions of the domain corresponded to those of the Merkle-Deutsch (1992) flat plate experimental configuration to facilitate comparison of the results.

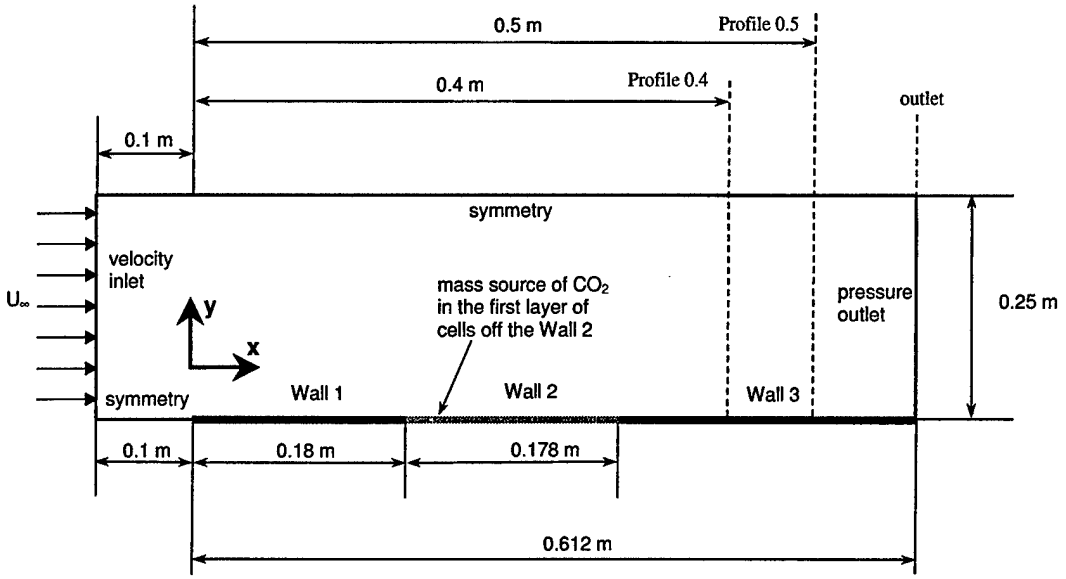

Figure 1. Schematic diagram of the computational domain.

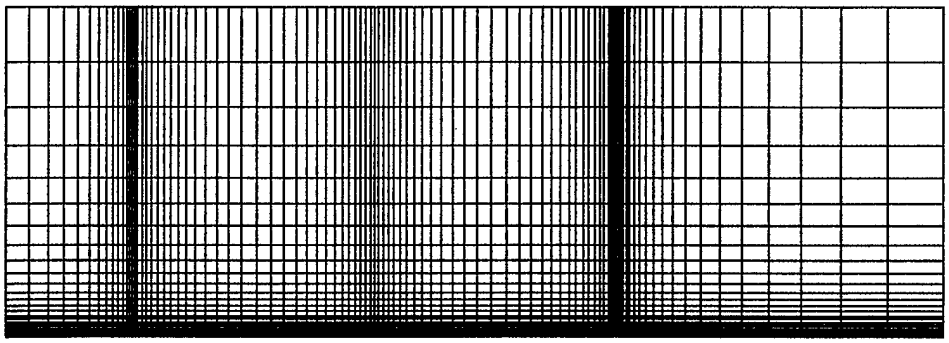

Figure 2. The 112 x 64 computational grid.

Seven gas input flow rates and two free stream velocities were modeled to study the effect of mixture density variation along with the reference cases with no bubbles. The input conditions for computed cases are summarized in Table 1.

To validate that the computational grid satisfied $y^+ \leq 1$ at the first cell of the wall, the y^+ at the first cell was plotted along the flat plate for all computational cases. A sample plot for case Q3 with free stream velocity of 10.9 m/s is shown in Figure 3. The y^+ values along the flat plate for other studied cases had similar values and are not presented here.

Table 1.
Input conditions of computational cases

Case	CO_2 Volume Flow Rate, m^3/s	Nondimensional Flow Rate, $Q/U_\infty A$	Free Stream Velocity, m/s	Re_L based on the total plate length
Q0-V10	0	0	10.9	6.67×10^6
Q1-V10	0.0005	0.0025	10.9	6.67×10^6
Q2-V10	0.001	0.005	10.9	6.67×10^6
Q3-V10	0.002	0.01	10.9	6.67×10^6
Q4-V10	0.003	0.015	10.9	6.67×10^6
Q5-V10	0.004	0.02	10.9	6.67×10^6
Q6-V10	0.005	0.025	10.9	6.67×10^6
Q7-V10	0.006	0.03	10.9	6.67×10^6
Q0-V4	0	0	4.2	2.57×10^6
Q1-V4	0.0002	0.0025	4.2	2.57×10^6
Q2-V4	0.0004	0.005	4.2	2.57×10^6
Q5-V4	0.0015	0.02	4.2	2.57×10^6
Q7-V4	0.0023	0.03	4.2	2.57×10^6

In order to validate the model further, simulated boundary layer velocity profile for the case without gas injection was compared to standard law-of-the-wall curves. Boundary layer velocity profile in the outlet plain of the computational domain is plotted in Figure 4 in inner variables and compared to the standard curves. It is seen from the figure that the simulated profile is in good agreement with standard curves.

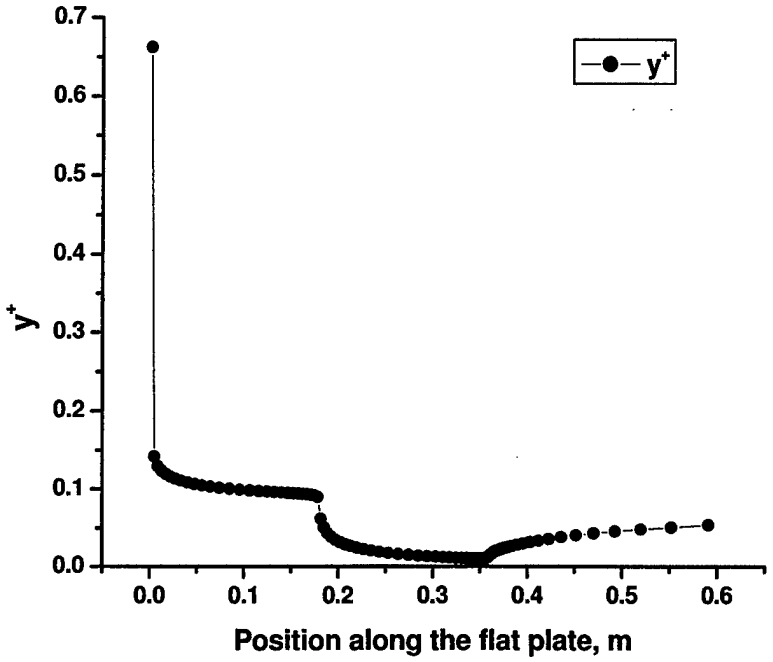

Figure 3. The y^+ in the first cell of the wall along the flat plate for case of Q3 and U_∞=10.9 m/s.

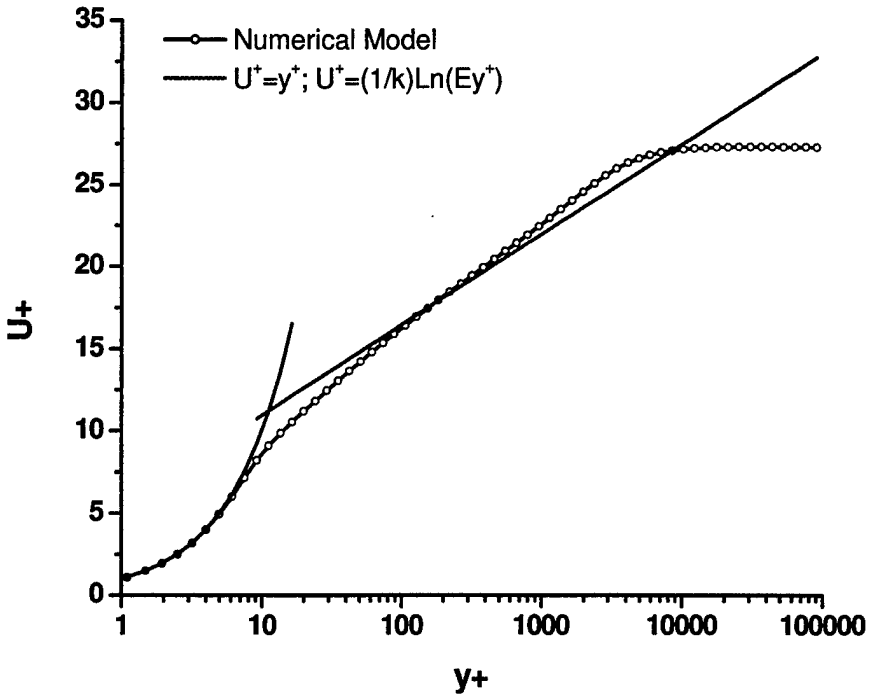

Figure 4. Comparison of simulated boundary layer velocity profile with standard law of the wall curves.

Figure 5 compares computed drag reduction with the experimental data of Merkle and Deutsch (1992) and with the ensemble averaged multifield two-fluid modeling results of Kunz et al. (2003). In this figure, the plate drag coefficient normalized by the single-phase drag coefficient is plotted versus nondimensional gas injection flow rate. The figure shows not only that the results of the current model are close to those of the more advanced model of Kunz et al. but also that the current model correctly predicts smaller drag reduction for lower free stream velocity as observed in the experiments.

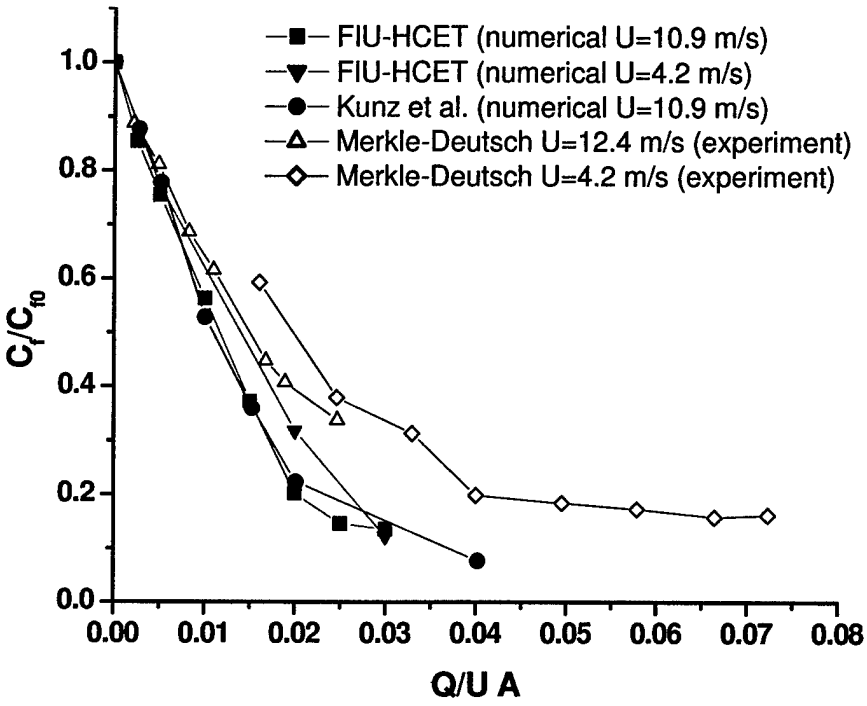

Figure 5. Comparison of the computed plate drag coefficient with the experimental data of Merkle and Deutsch (1992) and the numerical model of Kunz et al. (2003).

3.0 DENSITY RATIO EFFECT

A parametric study of density ratio effect on drag reduction was carried out. Density ratio is defined as the ratio of density of water to that of injected gas. To perform this study, the density of CO_2 gas was varied in the range from 1 kg/m^3 to 200 kg/m^3; all other material properties of CO_2 were not changed. Table 2 summarizes studied input parameter values.

Table 2.
Input parameters for density ratio effect studies

Density Ratio	Gas Flow Rate, $Q/U_\infty A$	Free Stream Velocity, m/s
1000 559 333 250 125 50 30 10 5	0.005 0.02	10.9

In order to investigate the effect of density ratio on microbubble drag reduction, one has to ensure that the volumetric concentrations of injected gas are identical for different density ratio values. Figure 6 shows volumetric concentration profiles for different density ratios at two vertical profiles above the flat plate. These profiles are designated as "outlet" and "profile 0.4" in Figure 1. The free stream velocity and nondimensional gas flow rate for all the cases shown in Figure 6 were the same and equal to 10.9 m/s and 0.005, respectively.

To quantify the difference between the concentration profiles, they were plotted versus the average concentration profile along with ± 5% deviations from it as shown in Figures 7 and 8. It is seen from Figures 7 and 8 that all the profiles at the "Outlet" and "Profile 0.4" positions are within 5% of the average profile. This indicates that presented simulation cases can be used to investigate the effect of density ratio on the microbubble drag reduction.

In a similar fashion, Figure 9 shows gas volumetric concentration profiles for different density ratios at "Outlet" position for the cases with free stream velocity of 10.9 m/s and nondimensional gas flow rate of 0.02. Figure 10 shows concentration profiles plotted versus the average concentration profile along with ± 5% deviations from average profile. Figure 10 shows that for nondimensional gas flow rate of 0.02 gas volumetric concentration profiles are within 5% of the average profile, and thus the simulation cases can be used for density ratio effect study.

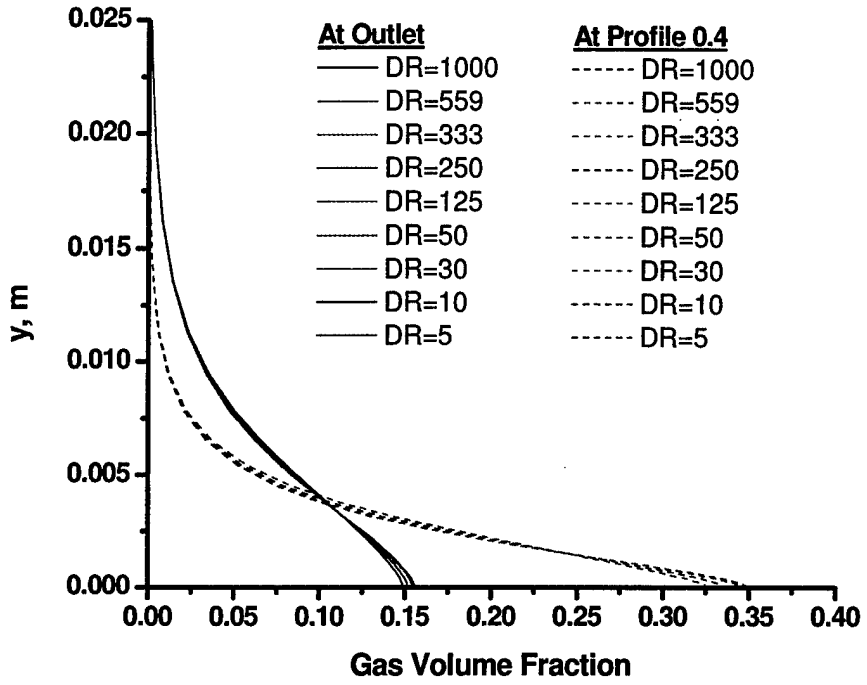

Figure 6. Computed gas volume fraction profiles in the boundary layer at two vertical profiles above the flat plate (U=10.9 m/s, $Q/U_\infty A = 0.005$).

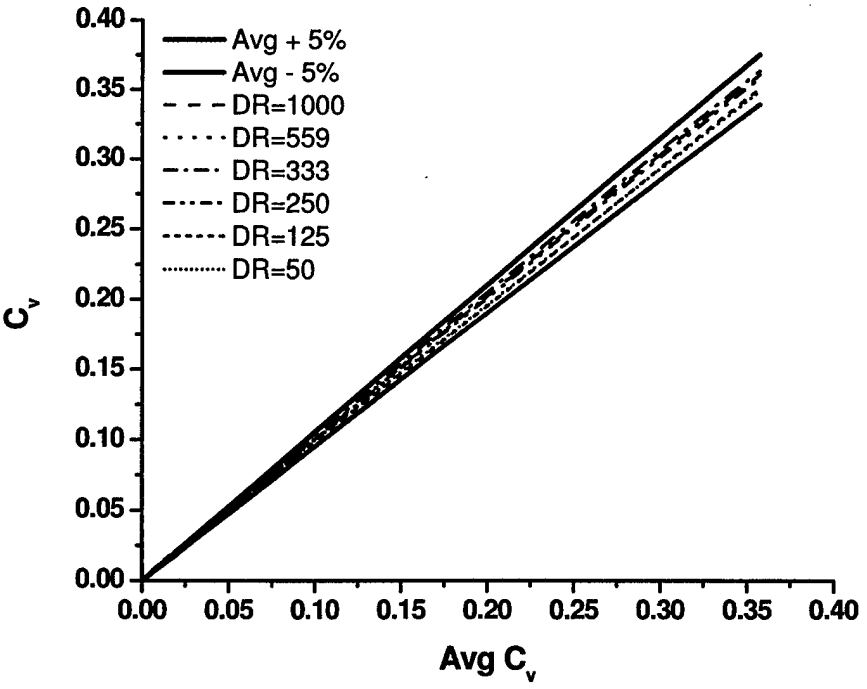

Figure 7. Comparison of gas volume concentration profiles at "Profile 0.4" above the flat plate (U=10.9 m/s, $Q/U_\infty A = 0.005$).

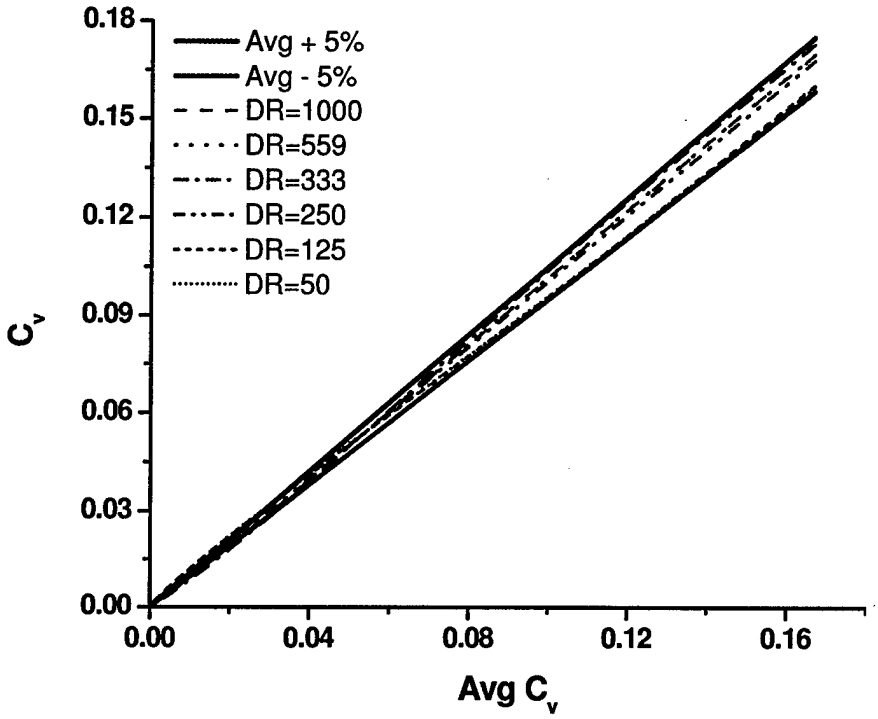

Figure 8. Comparison of gas volume concentration profiles at "Outlet" above the flat plate (U=10.9 m/s, $Q/U_\infty A = 0.005$).

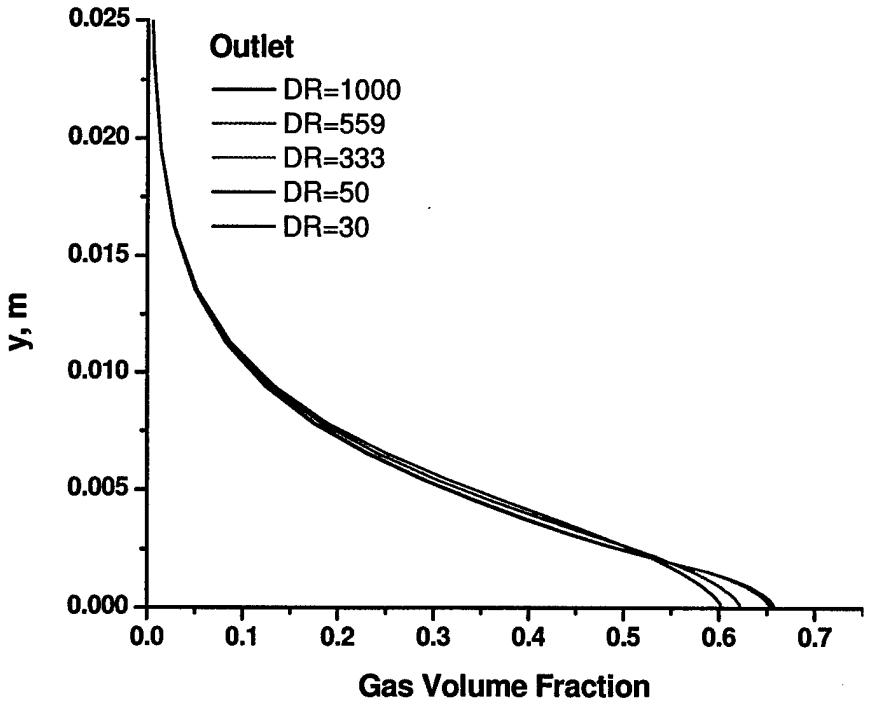

Figure 9. Computed gas volume fraction profiles in the boundary layer at "Outlet" vertical profile above the flat plate (U=10.9 m/s, $Q/U_\infty A = 0.02$).

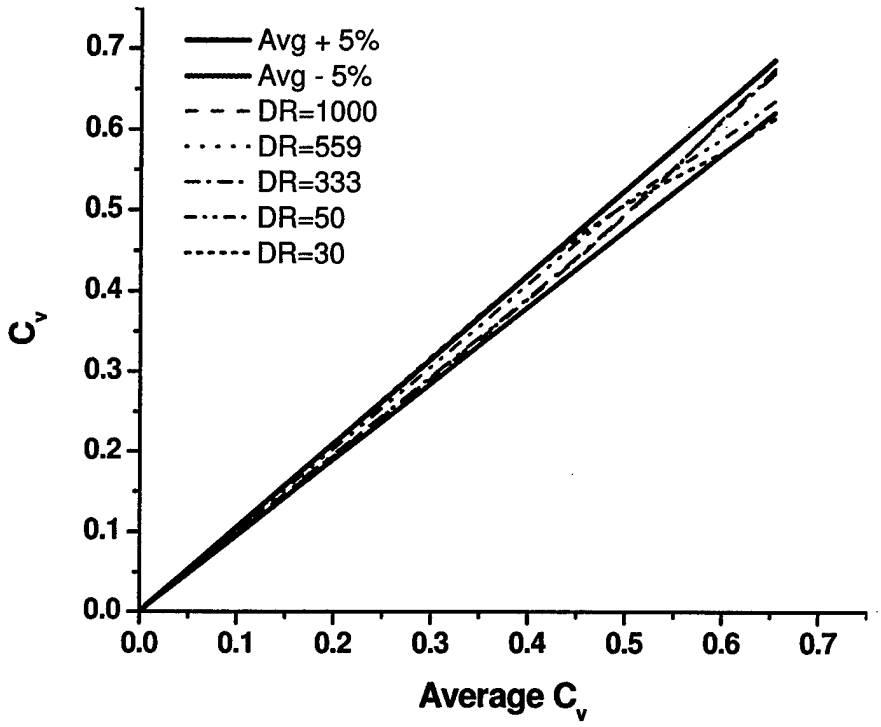

Figure 10. Comparison of gas volume concentration profiles at "Outlet" above the flat plate (U=10.9 m/s, $Q/U_\infty A = 0.02$).

Effect of density ratio on velocity profiles in the outlet of the computational domain is shown in Figure 11 for cases with nondimensional gas flow rate of 0.005. As seen from Figure 11, the velocity profiles for all density ratios except DR=5 are practically identical. The velocity profile for DR=5 has slightly lower gradient for 1 mm < y < 10 mm than the rest of the profiles.

Effect of density ratio on the drag coefficient is shown in Figure 12. On this figure, drag coefficient value for DR=1 ($\rho_{gas} = \rho_{water}$) is taken as that of single-phase flow with no gas injection. From Figure 12 it is seen that for low gas injection rate ($Q/U_\infty A = 0.005$) with increasing density ratio, drag coefficient quickly decreases from its single-phase flow value and remains almost unchanging for density ratios between 5 and 1000. The drag coefficient for DR=5 is only about 1% higher than that for DR=1000. For high gas injection flow rate ($Q/U_\infty A = 0.02$), a gradual decrease of the drag coefficient with increasing density ratio is observed, which indicates that simple mixture density variation effect plays one of the major roles in microbubble drag reduction phenomenon.

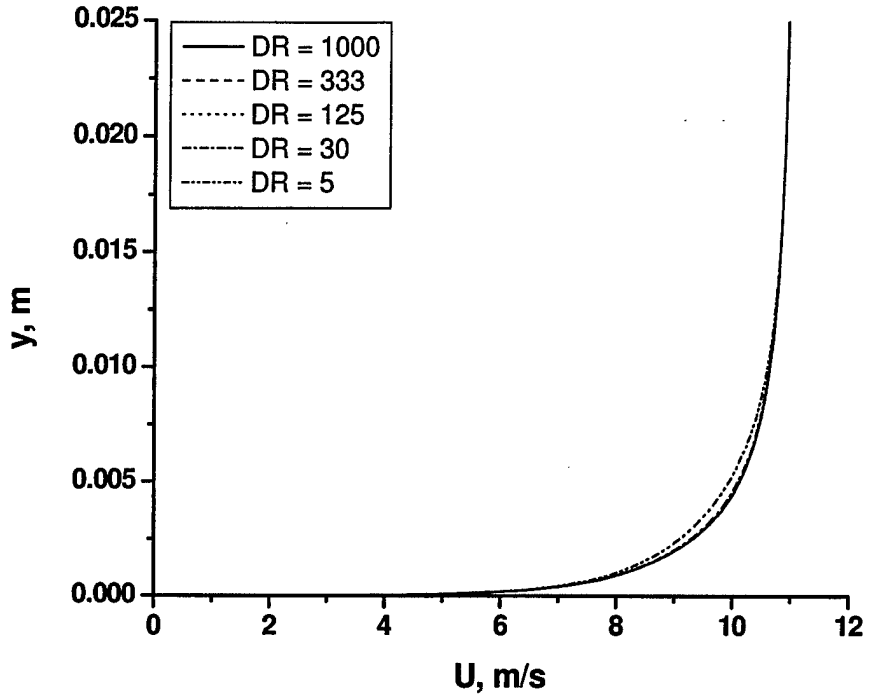

Figure 11. Computed velocity profiles in the boundary layer at "Outlet" vertical profile above the flat plate (U=10.9 m/s, $Q/U_\infty A$ = 0.005).

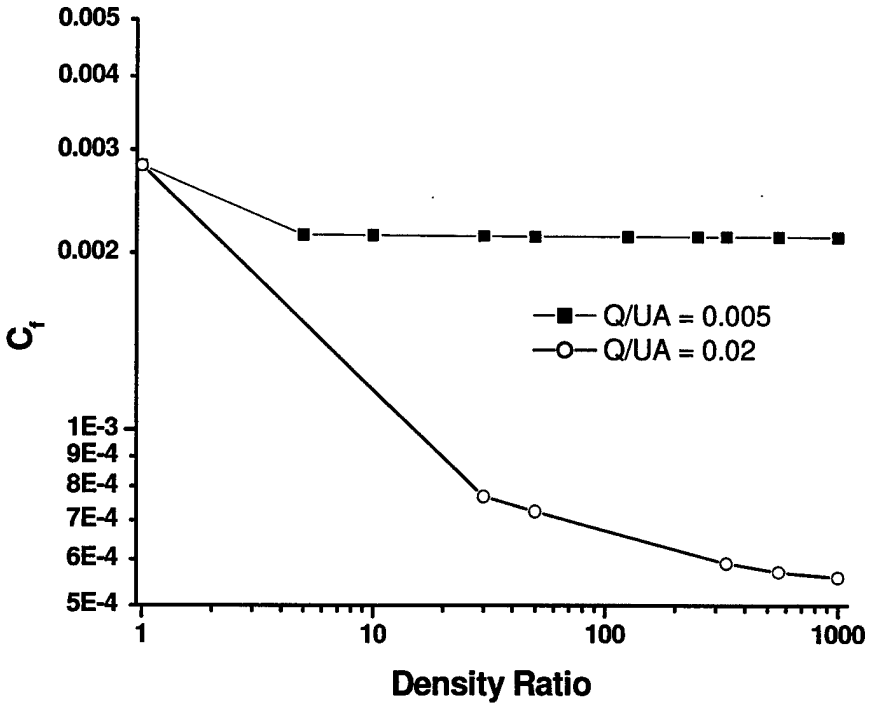

Figure 12. Density ratio effect on the drag coefficient (U=10.9 m/s, $Q/U_\infty A$ = 0.02 and 0.005).

4.0 SURFACE ROUGHNESS EFFECT

Assessments of the role of surface roughness in microbubble drag reduction were performed using the same numerical model. Surface roughness was included in the model described in Section 2 using the equivalent sand grain roughness method. In this method roughness height in inner variables is defined as

$$k_s^+ = \max\left(1.0, \frac{\rho k_s u_\tau}{\mu}\right) \tag{11}$$

Next, the value of ω at the wall is specified as

$$\omega_w = \frac{\rho u_\tau^2}{\mu}\omega^+ \tag{12}$$

where ω^+ in the laminar sublayer is given by

$$\omega^+ = \min\left(\omega_w^+, \frac{6}{\beta_\infty^*\left(y^+\right)^2}\right), \text{ where } \omega_w^+ = \begin{cases} \left(\frac{50}{k_s^+}\right)^2 & k_s^+ < 25 \\ \frac{100}{k_s^+} & k_s^+ \geq 25 \end{cases} \tag{13}$$

Roughness heights k_s of 75 μm and 150 μm were used in the simulation cases with free stream velocity of 10.9 m/s and nondimensional gas injection flow rate of 0.02. The input parameters as well as calculated drag coefficients are summarized in Table 3.

It is seen from Table 3 that with increasing roughness height, the HCET single-phase model predicts increasing drag coefficient for the cases without gas injection as well as for the cases with gas injection. It is known from the experiments that microbubble concentration reaches maximum slightly above the flat plate (Merkle and Deutsch 1992), while near the plate the bubble concentration is almost zero. Due to this fact, HCET performed a series of simulations where mixture viscosity near the wall was replaced with water viscosity in the thin layer above the flat plate. The input conditions and result of these simulations are shown in the bottom rows of Table 3. The table shows that with increasing height of the layer where mixture viscosity is replaced by that of water, the drag coefficient is decreasing; however, the drag coefficient value is still higher than that for smooth surface case.

Figures 13 and 14 show the effect of roughness on velocity and gas concentration profiles in the outlet of the computational domain. It is seen from Figure 13 that roughness effect on the gas concentration is very minor and confined to the boundary layer. With increasing roughness, the gas concentration near the flat plate is decreasing (y < 1mm), while further above the plate (y > 1mm) it is increasing. Roughness effect on velocity profiles is also small and limited to the boundary layer as seen from Figure 14. With increasing roughness, velocity gradient near the flat plate is decreasing.

To quantify the amount of drag reduction achieved by introduction of microbubbles, the drag coefficient for the case with bubbles was nondimensionalized by its value for the case without bubbles obtained for the same roughness height. The results are presented in Figure 15. The figure indicates that increased drag reduction is obtained with increased

surface roughness. The same trend was observed in recent experiments at the Applied Research Laboratory at Penn State (Deutsch et al. 2003).

Table 3.
Input parameters and results of surface roughness effect studies

Roughness Height, μm	Gas Flow Rate, $Q/U_\infty A$	Free Stream Velocity, m/s	Viscosity	Drag Coefficient
0	0	10.9	water	0.002826272
0	0.02	10.9	mixture	0.000571554
75	0	10.9	water	0.005405200
75	0.02	10.9	mixture	0.000646687
150	0	10.9	water	0.008695437
150	0.02	10.9	mixture	0.000800603
150	0.02	10.9	water, y<0.2 mm mixture y>0.2mm	0.000794396
150	0.02	10.9	water, y<0.5 mm mixture y>0.5mm	0.00076992
150	0.02	10.9	water, y<1 mm mixture y>1 mm	0.000734048

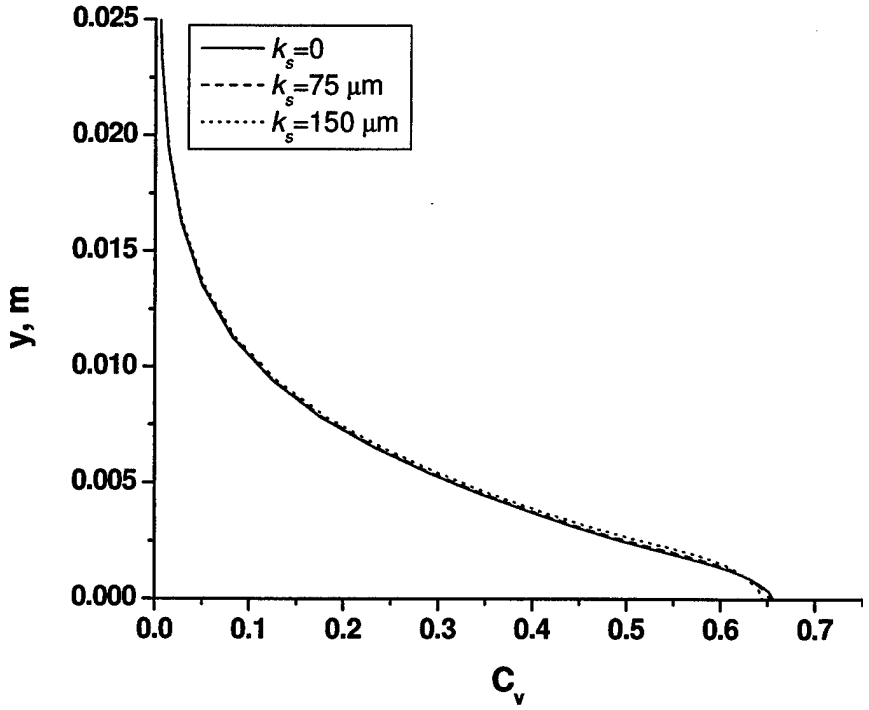

Figure 13. Surface roughness effect on gas concentration profiles.

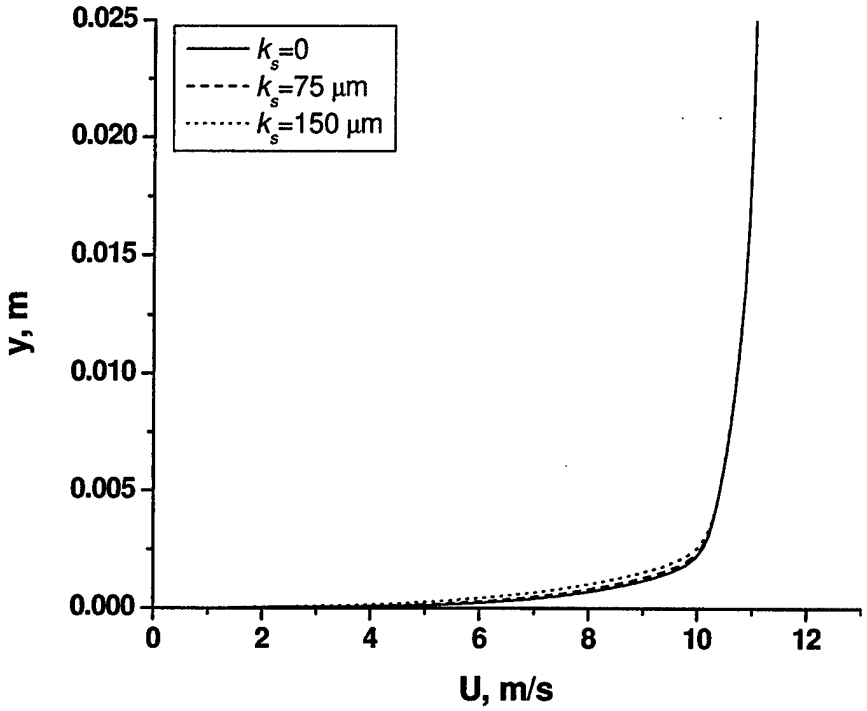

Figure 14. Surface roughness effect on velocity profiles.

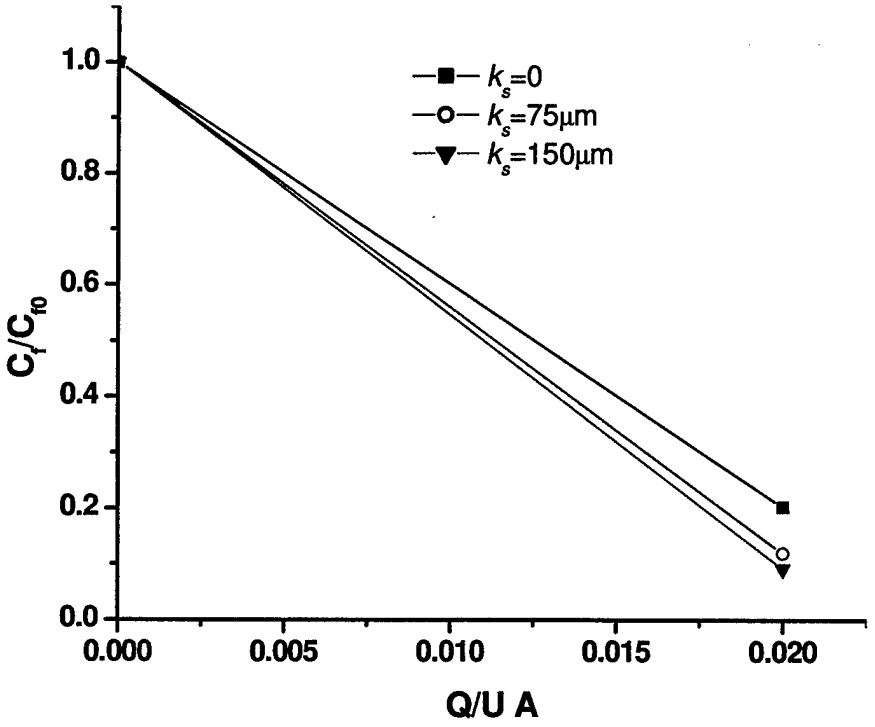

Figure 15. Surface roughness effect on the microbubble drag reduction.

5.0 CONCLUSIONS

Major conclusions from the performed numerical simulation study are summarized below:

- Single-phase model with bubbles introduced as species mass source was able to predict drag reduction consistent with experimental data and more complex two-fluid model results.
- For low gas injection flow rates
  - Drag reduction was predicted even for the smallest studied density ratio.
  - Drag coefficient remained almost unchanging for density ratios between 5 and 1000.
- For high gas injection flow rates, gradual decrease of the drag coefficient with increasing density ratio was predicted, which indicates that simple mixture density variation effect plays a very important, if not major, role in microbubble drag reduction phenomenon.
- Replacing mixture viscosity with water viscosity in the thin layer above the flat plate caused model to predict lower drag coefficient; however, this drag coefficient is still higher than that of smooth surface.
- Single-phase model correctly predicted experimentally observed increasing drag reduction with increasing surface roughness.

Acknowledgement

Research team members of this project are grateful to the Technical Representative Dr. Robert F. Kunz for guidance, helpful discussions, and encouragement throughout the entire project duration and for making this project possible through financial support.

Nomenclature

Symbols

A	Area, m^2
C_f	Drag coefficient, dimensionless
DR	$= \frac{\rho_{water}}{\rho_{gas}}$ Density ratio, dimensionless
k_s	roughness height, m
p	Pressure, Pa
Q	Flow rate, m^3/s
Re	Reynolds number, dimensionless
t	Time, s

U_∞ Free-stream velocity, m/s

u_i mean velocity components (i = 1, 2, 3), m/s

u'_i fluctuating velocity components (i = 1, 2, 3), m/s

u_τ $= \sqrt{\frac{\tau_w}{\rho}}$ friction velocity, m/s

u^+ $= \frac{u}{u_\tau}$ velocity in inner variables, dimensionless

y wall normal coordinate, m

y^+ $= \frac{\rho u_\tau y}{\mu}$ wall normal coordinate in inner variables, dimensionless

μ Dynamic viscosity, Pa-s

ρ Density, kg/m^3

τ_w wall shear stress, Pa

References

Deutsch, S., Moeny, M., Fontaine, A., and Petrie, H. (2003). Microbubble Drag Reduction in Rough Walled Turbulent Boundary Layers. 4th ASME–JSME Joint Fluids Engineering Conference, Honolulu, Hawaii, July 6–11, 2003, Paper N FED2003-45647.

Kim, S.-Y., and Cleaver, J.W. (1995). The persistence of drug reduction following the injection of microbubbles into a turbulent boundary layer. International Communications in Heat and Mass Transfer, 22(3), 353-357.

Kunz, R.F., Deutsch, S., and Lindau, J.W. (2003). Two Fluid Modeling of Microbubble Turbulent Drag Reduction. 4th ASME–JSME Joint Fluids Engineering Conference, Honolulu, Hawaii, July 6–11, 2003, Paper N FED2003-45640.

Kunz, R.F. (2003). Private Communication.

Legner, H.H. (1984). A simple model for gas bubble drag reduction. Physics of Fluids, 27(12), 2788-2790.

Madavan, N.K., Merkle, C.L., and Deutsch, S. (1985). Numerical investigations into the mechanisms of microbubble drag reduction. Journal of Fluids Engineering, 107, 370-377.

Marie, J.L. (1987). Simple Analytical Formulation For Microbubble Drag Reduction. PhysicoChemical Hydrodynamics , 8(2), 213-220 .

McCormick, M.E., and Bhattacharya, R. (1973). Drag reduction of a submersible hull by electrolysis. Naval Eng. J., 85, 11-16.

Meng, J.C.S., and Uhlman, J.S., Jr. (1998). Microbubble formation and splitting in a turbulent boundary layer for turbulence reduction. Proceedings of the International Symposium on Seawater Drag Reduction, 22-23 July 1998, 341-355.

Merkle, C.L., and Deutsch, S. (1992). Microbubble Drag Reduction in Liquid Turbulent Boundary Layers. Applied Mechanics Reviews, 45(3), 103-127.

Wilcox, D.C. (1998). Turbulence Modeling for CFD. DCW Industries, Inc., La Canada, California.

Xu, J., Maxey, M.R., and Karniadakis, G.E. (2002). Numerical simulation of turbulent drag reduction using micro-bubbles. Journal of Fluid Mechanics, 468, 271-281.